

An efficient implementation of high-order coupled-cluster techniques applied to quantum magnets

Chen Zeng*, D.J.J. Farnell, and R.F. Bishop†

Department of Physics, University of Manchester Institute of Science and Technology (UMIST),

P.O. Box 88, Manchester M60 1QD, United Kingdom

(September 20, 2018)

Keywords: coupled-cluster method, quantum magnets, strongly correlated spin lattices, high-order LSUB m approximations, generalised Néel model state, square lattice XXZ model, triangular lattice Heisenberg antiferromagnet, ket-state parametrisation, bra-state parametrisation, lattice animals and fundamental configurations, ground-state energy, sublattice magnetisation, anisotropy susceptibility, critical points, quantum order, quantum phase transitions.

We illustrate how the systematic inclusion of multi-spin correlations of the quantum spin-lattice systems can be efficiently implemented within the framework of the coupled-cluster method by examining the ground-state properties of both the square-lattice and the frustrated triangular-lattice quantum antiferromagnets. Various physical quantities including the ground-state energy, the anisotropy susceptibility, and the sublattice magnetisation are calculated and compared with those obtained from such other methods as series expansions and quantum Monte Carlo simulations.

I. INTRODUCTION

The techniques now available in the field of *ab initio* quantum many-body theory have become increasingly refined over the last decade or so. This is particularly true for what is nowadays recognised as one of the most powerful modern techniques, namely, the coupled-cluster method (CCM)^{1–9}. The results obtained from the CCM have become fully competitive with series expansions, variational calculations and quantum Monte Carlo (QMC) simulations (for the cases in which QMC may be applied).

Quantum magnets not only provide useful models of many physically realisable magnetic systems but also serve as prototypical models of quantum many-body systems. Their rich phase diagrams due to strong quantum effects have naturally provided an excellent test-bed where the above-mentioned methods can be applied and further refined. One example demonstrating rich and initially unexpected behaviour is provided by the Haldane conjecture¹⁰, which states that the one-dimensional (1D) spin-1 Heisenberg antiferromagnet (HAF) possesses an excitation gap, in sharp contrast to its spin- $\frac{1}{2}$ counterpart. This was surprising at the time because conventional spin-wave theory predicts a gapless excitation spectrum regardless of spin magnitude. However, the Haldane conjecture has subsequently been confirmed by numerical calculations¹¹. Moreover, in the aftermath of the discovery of the superconducting cuprates, much effort has been devoted to uncovering such subtle effects as spin-nematic, spin-Peierls and chiral spin liquid orderings in two-dimensional (2D) quantum antiferromagnets, among which the frustrated quantum antiferromagnets on the triangular and the Kagomé lattices have recently attracted considerable theoretical attention^{12–21}.

The CCM has been applied to various quantum magnets over the past six years. The first application of the CCM to these systems was performed by Roger and Hetherington²², who obtained good results at low levels of approximation for the ground-state energy of both the 1D chain and the 2D square-lattice HAF, and also for solid ³He where ring exchanges of nuclear spins are considered. Since then the CCM has been applied to the isotropic (Heisenberg) and anisotropic HAF (or XXZ model) in 1D and on the 2D square lattice, both for spin- $\frac{1}{2}$ ^{23–26} systems and higher spins systems^{27,28}; to the spin-1 Heisenberg-biquadratic model²⁹; and to such *frustrated* spin models as the spin- $\frac{1}{2}$ J_1 - J_2 (or Majumdar-Ghosh) model^{30–32} and the 2D triangular lattice HAF^{33,34}. It has also been applied to the spin-1 easy-plane ferromagnet³⁵. Among these, Bishop *et al.*^{23,29} not only put forth several systematic *localised* approximation schemes to perform higher-order calculations yielding good results on the ground-state sublattice magnetisations and approximate excitation spectra, but also used an infinite-order, two-body approximation scheme to obtain evidence of a zero-temperature quantum phase transitions. Moreover, the systematic inclusion of spin-spin correlations based on a *dimerised* state has also been made possible within the framework of the CCM^{31,36}, to study spin-Peierls ordering. This may provide a possible inroad to probe more subtle topological order in the absence of *solid* order, as in the case of the chiral spin liquid^{12,17}. The quantitative description of such phases remains one of the most challenging problems for modern microscopic quantum many-body theory in general, and the CCM in particular.

More recently, attention has been given to extending the CCM calculations to higher orders²⁶ in the particular case of the XXZ model, by using a *localised* approximation scheme, and by taking into account multi-spin correlations on up to 10 contiguous lattice sites in 1D and on up to 6 contiguous lattice sites in 2D. The ground-state energies, for example, are found to be in excellent agreement (i.e., within about 0.03%) with the exact result in 1D, and with

those obtained from spin-wave theory³⁷, series expansion³⁸ and QMC calculations^{39,40} in 2D. However, it is fair to say that in 2D, to achieve the same accuracy on other more interesting physical quantities such as the ground-state sublattice magnetisation and the excitation spectrum, and to further clarify the nature of zero-temperature quantum phase transitions, the inclusion of multi-spin correlations of still higher orders is clearly needed. Since the extent of the task of determining the CCM equations and solving them grows extremely rapidly with the approximation level, efficient algorithms for performing the CCM calculations thus become indispensable³⁴.

The motivation of the present work is two-fold: (1) we analyse in detail the computational aspects of the CCM in the context of quantum antiferromagnets, in order to devise an efficient implementation and to show how the systematic inclusion of multi-spin correlations can be made simple; and (2) we revisit the spin- $\frac{1}{2}$ quantum antiferromagnets on both the square and the triangular lattices by utilising this algorithm in a way which now enables us to increase the number of independent and *localised* multi-spin configurations to be considered by at least an order of magnitude over previous calculations. In this article we focus on the above two models in the regimes where a Néel-like order represents the corresponding classical limit. The present method, however, should be of general utility to quantum magnets where a spin-Peierls order is relevant, for example.

A brief description of the contents of this article now follows. In Sec. II we describe how a reformulation of the CCM problem has been achieved. The characteristic CCM similarity transform of the spin operators is evaluated at a very general approximation level, and the Hamiltonian is reformulated purely in terms of spin-raising operators for a spin- $\frac{1}{2}$ system. We also show that the form of the new Hamiltonian easily lends itself to a localised set of approximations called the LSUB m scheme. In so doing the CCM technique is itself clarified. The computational method used to determine our fundamental set of configurations within this approximation scheme is described, and the derivation of the resulting CCM equations is discussed in detail. The method is then applied to the square-lattice spin- $\frac{1}{2}$ XXZ antiferromagnet, and the triangular-lattice spin- $\frac{1}{2}$ anisotropic antiferromagnet¹⁵ in Secs. III and IV respectively. Our conclusions are given in Sec. V, where we also discuss possibilities for further extending our computational solution to even higher-order calculations by making use of parallel processing and other strategies.

II. THE CCM FORMALISM FOR SPIN-LATTICE MODELS

A. Basic Ingredients of the CCM

Since detailed descriptions of the fundamentals of the CCM are available in the literature¹⁻⁹, we only highlight the essential ingredients of its application here. The exact ket and bra ground-state energy eigenvectors, $|\Psi\rangle$ and $\langle\tilde{\Psi}|$, of a many-body system described by a Hamiltonian H ,

$$H|\Psi\rangle = E_g|\Psi\rangle; \quad \langle\tilde{\Psi}|H = E_g\langle\tilde{\Psi}|, \quad (1)$$

are parametrised within the single-reference CCM as follows:

$$\begin{aligned} |\Psi\rangle &= e^S|\Phi\rangle; \quad S = \sum_{I \neq 0} s_I C_I^+, \\ \langle\tilde{\Psi}| &= \langle\Phi|\tilde{S}e^{-S}; \quad \tilde{S} = 1 + \sum_{I \neq 0} \tilde{s}_I C_I^-. \end{aligned} \quad (2)$$

The single model or reference state $|\Phi\rangle$ is required to have the property of being a cyclic vector with respect to two well-defined Abelian subalgebras of *multi-configurational* creation operators $\{C_I^+\}$ and their Hermitian-adjoint destruction counterparts $\{C_I^- \equiv (C_I^+)^\dagger\}$. Thus, $|\Phi\rangle$ plays the role of a vacuum state with respect to a suitable set of (mutually commuting) many-body creation operators $\{C_I^+\}$,

$$C_I^-|\Phi\rangle = 0, \quad I \neq 0, \quad (3)$$

with $C_0^- \equiv 1$, the identity operator. These operators are complete in the many-body Hilbert (or Fock) space,

$$1 = |\Phi\rangle\langle\Phi| + \sum_{I \neq 0} C_I^+|\Phi\rangle\langle\Phi|C_I^-. \quad (4)$$

Also, the *correlation operator* S is decomposed entirely in terms of these creation operators $\{C_I^+\}$, which, when acting on the model state ($\{C_I^+|\Phi\rangle\}$), create excitations about the model state. We note that although the manifest

Hermiticity, ($\langle \tilde{\Psi} |^\dagger = |\Psi\rangle / \langle \Psi | \Psi \rangle$), is lost, the intermediate normalisation condition $\langle \tilde{\Psi} | \Psi \rangle = \langle \Phi | \Psi \rangle = \langle \Phi | \Phi \rangle \equiv 1$ is explicitly imposed. The *correlation coefficients* $\{s_I, \tilde{s}_I\}$ are regarded as being independent variables, even though formally we have the relation,

$$\langle \Phi | \tilde{S} = \frac{\langle \Phi | e^{S^\dagger} e^S}{\langle \Phi | e^{S^\dagger} e^S | \Phi \rangle} . \quad (5)$$

The full set $\{s_I, \tilde{s}_I\}$ thus provides a complete description of the ground state. For instance, an arbitrary operator A will have a ground-state expectation value given as,

$$\bar{A} \equiv \langle \tilde{\Psi} | A | \Psi \rangle = \langle \Phi | \tilde{S} e^{-S} A e^S | \Phi \rangle = \bar{A}(\{s_I, \tilde{s}_I\}) . \quad (6)$$

We note that the exponentiated form of the ground-state CCM parametrisation of Eq. (2) ensures the correct counting of the *independent* and excited correlated many-body clusters with respect to $|\Phi\rangle$ which are present in the exact ground state $|\Psi\rangle$. It also ensures the exact incorporation of the Goldstone linked-cluster theorem, which itself guarantees the size-extensivity of all relevant extensive physical quantities. One crucial difference between the CCM parametrisation of the ground state and those used in spin-wave³⁷ and variational Monte Carlo calculations⁴¹ is that although they all adopt an exponentiated form, the former (CCM) contains spin-raising operators only.

The determination of the correlation coefficients $\{s_I, \tilde{s}_I\}$ is achieved by taking appropriate projections onto the ground-state Schrödinger equations of Eq. (1). Equivalently, they may be determined variationally by requiring the ground-state energy expectation functional $\bar{H}(\{s_I, \tilde{s}_I\})$, defined as in Eq. (6), to be stationary with respect to variations in each of the (independent) variables of the full set. We thereby easily derive the following coupled set of equations,

$$\delta \bar{H} / \delta \tilde{s}_I = 0 \Rightarrow \langle \Phi | C_I^- e^{-S} H e^S | \Phi \rangle = 0, \quad I \neq 0 ; \quad (7)$$

$$\delta \bar{H} / \delta s_I = 0 \Rightarrow \langle \Phi | \tilde{S} e^{-S} [H, C_I^+] e^S | \Phi \rangle = 0, \quad I \neq 0 . \quad (8)$$

Equation (7) also shows that the ground-state energy at the stationary point has the simple form

$$E_g = E_g(\{s_I\}) = \langle \Phi | e^{-S} H e^S | \Phi \rangle . \quad (9)$$

It is important to realize that this (bi-)variational formulation does *not* lead to an upper bound for E_g when the summations for S and \tilde{S} in Eq. (2) are truncated, due to the lack of exact Hermiticity when such approximations are made. However, it is clear that the important Hellmann-Feynman theorem *is* preserved in all such approximations.

We also note that Eq. (7) represents a coupled set of nonlinear polynomial equations for the c -number correlation coefficients $\{s_I\}$. The nested commutator expansion of the similarity-transformed Hamiltonian,

$$\hat{H} \equiv e^{-S} H e^S = H + [H, S] + \frac{1}{2!} [[H, S], S] + \dots , \quad (10)$$

together with the fact that all of the individual components of S in the sum in Eq. (2) commute with one another, imply that each element of S in Eq. (2) is linked directly to the Hamiltonian in each of the terms in Eq. (10). Thus, each of the coupled equations (7) is of linked cluster type. Furthermore, each of these equations is of finite length when expanded, since the otherwise infinite series of Eq. (10) will always terminate at a finite order, provided (as is usually the case) that each term in the second-quantised form of the Hamiltonian H contains a finite number of single-body destruction operators, defined with respect to the reference (vacuum) state $|\Phi\rangle$. Therefore, the CCM parametrisation naturally leads to a workable scheme which can be efficiently implemented computationally. It is also important to note that at the heart of the CCM lies a similarity transformation, in contrast with the unitary transformation in a standard variational formulation in which the bra state $\langle \tilde{\Psi} |$ is simply taken as the explicit Hermitian adjoint of $|\Psi\rangle$.

B. Computational Aspects of the CCM for Spin-Lattice Models

1. Ket-State CCM Equations

In this section, the general formalism of the CCM outlined in the previous section will be henceforth applied to spin- $\frac{1}{2}$ quantum magnets with the emphasis on the common computational aspects involved in its implementation. Further model-specific details are deferred until Secs. III and IV.

To be specific, in this article we restrict ourselves to spin- $\frac{1}{2}$ quantum antiferromagnets in the regimes where the corresponding classical limit is described by a generalised Néel-like ordering, i.e., where all spins on each sublattice are separately aligned in the coordinates of a global quantisation axis. However, it is a simple task (see Secs. III and IV for details) to introduce a different local quantisation axis on each sublattice by a suitable spin-rotation transformation, such that the above Néel-like state becomes a fully aligned (“ferromagnetic”) configuration in the local spin coordinates. This “ferromagnetic” state, $|\Phi\rangle$, will be chosen as the uncorrelated CCM model state, where, in the local axes, all spins point along the respective negative z -axis,

$$|\Phi\rangle = \bigotimes_{i=1}^N |\downarrow\rangle_i; \text{ in the local quantization axes .} \quad (11)$$

The correlation operator S is then decomposed wholly in terms of sums of products of single spin-raising operators, $s_k^+ \equiv s_k^x + is_k^y$, again defined with respect to the local quantisation axes,

$$S = [i_1]s_{i_1}^+ + [i_1i_2]s_{i_1}^+s_{i_2}^+ + \dots, \quad (12)$$

where $[i_1]$, $[i_1i_2]$ and so on stand for the corresponding (symmetric) spin-correlation coefficients (recall $\{s_I\}$ in Sec. IIA) specified by the sets of site indices, $\{i_1\}$, $\{i_1, i_2\}$ and so on, on the regular lattices under consideration. Implicit summations over repeated indices are also assumed. According to Eq. (7), the spin-correlation coefficients in Eq. (12) are to be determined by a set of CCM nonlinear equations:

$$0 = \langle \Phi | s_{j_1}^- s_{j_2}^- \dots s_{j_M}^- e^{-S} H e^S | \Phi \rangle, \quad (13)$$

where $s_{j_1}^- s_{j_2}^- \dots s_{j_M}^-$ is the Hermitian conjugate of the corresponding multi-spin correlation string $s_{j_1}^+ s_{j_2}^+ \dots s_{j_M}^+$.

In practice we clearly need an approximation scheme to truncate the expansion of S in Eq. (12) to some finite or infinite subset of the full set of multi-spin configurations $\{I\}$. The three most commonly used truncation methods up till now are: (1) the SUB n scheme, in which all correlations involving only n or fewer spins are retained, however far separated on the lattice; (2) the simpler SUB n - m sub-approximation, where only SUB n correlations spanning a range of no more than m adjacent lattice sites are retained; and (3) the systematic local LSUB m scheme, which includes all multi-spin correlations over all possible distinct locales on the lattice defined by m or fewer contiguous sites. Only the last approximation scheme will be adopted throughout this article.

The first step in the practical implementation of the LSUB m CCM is to enumerate all of the distinct multi-spin configurations or correlated clusters, which we shall henceforth call *fundamental* configurations, $\{i_1, i_2, \dots, i_n\}$ with $n \leq m$, retained in the LSUB m approximation. It should be noted that the multi-spin configurations that are related by Hamiltonian symmetries, translational and rotational alike, are counted as one single distinct configuration. Such a correlated cluster can be either a connected cluster of size m (also called a “lattice animal” or “polyomino”) or a subset of it (connected or disconnected). Although the asymptotic behaviour of the number of lattice animals on a regular lattice remains an open combinatorial question, efficient algorithms for enumerating lattice animals up to sizes of about 20 have been developed in various fields including percolation and cell growth problems⁴².

The second step in our modular implementation, namely, generating the corresponding set of CCM equations, is what we will focus on in the remainder of this section. Equation (13) reveals that there are essentially two computational aspects involved in obtaining all possible non-zero contributions to its right-hand side. The first is to calculate the similarity-transformed Hamiltonian which then acts on the model state, and the second is to select terms of the similarity-transformed Hamiltonian that match exactly the string of spin-lowering operators represented by the set of site indices $\{j_1, j_2, \dots, j_M\}$. The first aspect is intrinsically related to the noncommutative nature of quantum spin operators, and the second to the geometric considerations of the lattice on which the Hamiltonian is defined. We address these two aspects in more detail below.

The computation of the similarity-transformed Hamiltonian, $\hat{H} \equiv e^{-S} H e^S$, which acts on the model state $|\Phi\rangle$ can be performed straightforwardly by making use of the relations $s^-|\Phi\rangle = 0$ and $s^z|\Phi\rangle = -\frac{1}{2}|\Phi\rangle$. The goal here is to completely eliminate s^z and s^- , and thus retain the creation operators only, by utilising the commutation relations of the spin operators, namely, $[s^z, s^\pm] = \pm s^\pm$ and $[s^-, s^+] = -2s^z$. This greatly simplifies the matching problem in generating the CCM equations as discussed below. To this end, we note that the similarity-transformed single-spin operators can be expressed as:

$$\hat{s}_k^+ = s_k^+, \quad \hat{s}_k^z = s_k^z + F_k s_k^+, \quad \hat{s}_k^- = s_k^- - 2F_k s_k^z - (F_k)^2 s_k^+, \quad (14)$$

where $F_k \equiv \sum_l l[k i_1 \dots i_{l-1}] s_{i_1}^+ \dots s_{i_{l-1}}^+$. Furthermore, the commutation relations between the spin operators and the F_k operators can also be written in the following compact forms,

$$\begin{aligned}
[s_k^z, F_m] &= G_{km} s_k^+ , & [s_k^-, F_m] &= -2G_{km} s_k^z , \\
[s_k^z, (F_m)^2] &= 2F_m G_{km} s_k^+ , & [s_k^-, (F_m)^2] &= -2(G_{km})^2 s_k^+ - 4F_m G_{km} s_k^z ,
\end{aligned} \tag{15}$$

where $G_{km} \equiv \sum_l l(l-1)[kmi_1 \cdots i_{l-2}] s_{i_1}^+ \cdots s_{i_{l-2}}^+$. Unlike in previous equations, repeated indices in Eq. (15) *do not* imply summations. Clearly both F and G operators contain creation operators only. Consider then a typical two-spin interaction term, $s_k^- s_m^-$, for example, as contained in most spin-lattice Hamiltonians (see Sec. III and IV for a full description of the quantum spin Hamiltonians actually studied in this article). It is easy to prove the following relation:

$$\begin{aligned}
\hat{s}_k^- \hat{s}_m^- |\Phi\rangle &= \left(2(G_{km})^2 s_k^+ s_m^+ + 4F_k F_m G_{km} s_k^+ s_m^+ + (F_k)^2 (F_m)^2 s_k^+ s_m^+ \right) |\Phi\rangle \\
&\quad - \left(2G_{km} F_m s_m^+ + F_k (F_m)^2 s_m^+ + (F_k)^2 F_m s_k^+ + 2G_{km} F_k s_k^+ \right) |\Phi\rangle \\
&\quad + \left(G_{km} + F_k F_m \right) |\Phi\rangle .
\end{aligned} \tag{16}$$

In Eq. (16), the resulting terms from $\hat{s}_k^- \hat{s}_m^-$ are classified into three categories as explicitly containing both s_k^+ and s_m^+ , either s_k^+ or s_m^+ , and neither s_k^+ nor s_m^+ , respectively. The reason for such a classification will become clear when we consider the second aspect, namely, generating the CCM equations. Thus, the first case is the simplest of all three to deal with, since the site indices of all terms in the case, including both k and m , are completely fixed up to permutations by the *target* set $\{j_1, j_2, \cdots, j_M\}$ according to Eq. (13). Although, unlike in the first case, only one of k and m in the second case must lie within the set $\{j_1, j_2, \cdots, j_M\}$, the search for k or m in the matching problem can be easily performed once m or k is fixed. This comes about since the two-spin interactions with which we mostly deal are usually short-ranged. Typical examples are the nearest-neighbour interactions where k and m are simply the nearest neighbours as in the two models considered in this article. By contrast, neither index k nor index m in the last case must belong to the set $\{j_1, j_2, \cdots, j_M\}$. Nonetheless, for the LSUB m approximation scheme used here, both k and m must lie within a *finite* set of indices for which $\{j_1, j_2, \cdots, j_M\}$ is a subset.

To be more specific, let us consider the term in Eq. (16), $F_k F_m$, which can be written explicitly as:

$$F_k F_m = \sum_{l_1} \sum_{l_2} (l_1 + 1)(l_2 + 1) [ki_1 \cdots i_{l_1}] [mn_1 \cdots n_{l_2}] s_{i_1}^+ \cdots s_{i_{l_1}}^+ s_{n_1}^+ \cdots s_{n_{l_2}}^+ \tag{17}$$

where summation over repeated indices is implicitly assumed. Therefore, generating the part of the CCM equations due to this particular term $F_k F_m$ amounts to determining all possible non-zero contributions to $\langle \Phi | s_{j_1}^- \cdots s_{j_M}^- F_k F_m | \Phi \rangle$ according to Eq. (17). This is achieved by partitioning the target set $\{j_1, j_2, \cdots, j_M\}$ into two subsets $\{i_1 \cdots i_{l_1}\}$ and $\{n_1 \cdots n_{l_2}\}$ with $l_1 + l_2 = M$, followed by a search for the appropriate k and m in a *nearby* region that includes $\{i_1 \cdots i_{l_1}\}$ and $\{n_1 \cdots n_{l_2}\}$ respectively, such that both correlation coefficients $[ki_1 \cdots i_{l_1}]$ and $[mn_1 \cdots n_{l_2}]$ are the (symmetry-related) fundamental configurations of a given LSUB m approximation. Unlike earlier work^{22,23,26} where the maximum number of fundamental configurations is limited to 100 or so, the present approach based on partition completely eliminates the costly procedure implemented previously for avoiding double occupancies of spin- $\frac{1}{2}$ objects, and thus reduces the CPU usage a great deal. This optimal implementation becomes possible because all of the terms (e.g., $F_k F_m$) in the similarity-transformed Hamiltonian (\hat{H}) and, more importantly, their explicit structures are completely specified by the *seemingly tedious* reformulation of \hat{H} in terms of F_k , F_m and G_{km} operators. The CCM ket-state equations so obtained can then be solved by the standard Newton-Raphson method.

2. Bra-State CCM Equations

According to Eq. (6) in Sec. IIA, it is necessary to obtain both the ket-state correlation coefficients $\{s_I\}$ and the bra-state correlation coefficients $\{\tilde{s}_I\}$ in order to compute a general ground-state physical quantity such as the sublattice magnetisation. The task of generating the bra-state CCM equations (see Eq. (8)) turns out to be simple. Firstly, note that this set of coupled equations is linear in $\{\tilde{s}_I\}$, as is evident in Eq. (8); secondly, a simple equality, $\delta^2 \tilde{H} / \delta \tilde{s}_I \delta s_I = \delta^2 \tilde{H} / \delta s_I \delta \tilde{s}_I$, demonstrates that the bra-state equations can be readily generated from the already obtained CCM ket-state equations by appropriate differentiations.

Similarly, in the context of spin- $\frac{1}{2}$ quantum antiferromagnets, the \tilde{S} operator is in general decomposed entirely in terms of annihilation operators which are again defined with respect to local quantisation axes:

$$\tilde{S} = 1 + [\tilde{i}_1] s_{i_1}^- + [\tilde{i}_1 \tilde{i}_2] s_{i_1}^- s_{i_2}^- + \cdots , \tag{18}$$

where $[\widetilde{i}_1], [\widetilde{i}_1\widetilde{i}_2]$ and so on denote the corresponding bra-state spin-correlation coefficients (recall $\{s_I\}$ in Sec. IIA) specified by the sets of site indices $\{i_1\}, \{i_1, i_2\}$ and so on, which is the analogue of Eq. (12). Moreover, the same LSUB m truncation scheme is also adopted. This means that there exists a one-to-one mapping between the ket-state and the bra-state fundamental correlation coefficients which, to ease the burden of notation, are now denoted as $\{x_r\}$ and $\{\tilde{x}_r\}$ respectively. Now let $\delta\bar{H}/\delta\tilde{x}_r = P_r(x_1, x_2, \dots, \lambda) = 0$ denote the r^{th} ket-state CCM equation, which is given in terms of the ket-state correlation coefficients and λ , which stands for other parameters included in the Hamiltonian such as anisotropy, for example. Consequently \bar{H} may now be written in terms of $P_r(x_1, x_2, \dots, \lambda)$ and the bra-state correlation coefficients, $\{\tilde{x}_r\}$ as:

$$\bar{H} = P_0(x_1, x_2, \dots, \lambda) + \sum_{r=1}^{N_F} \tilde{x}_r P_r(x_1, x_2, \dots, \lambda) , \quad (19)$$

where $P_0(x_1, x_2, \dots, \lambda)$ denotes the zeroth-order CCM term, i.e., the ground-state energy expression, and N_F is the number of fundamental configurations retained for a given LSUB m approximation level. Therefore, the s^{th} bra-state equation may now be rewritten in terms of \tilde{x}_r and $P_r(x_1, x_2, \dots, \lambda)$:

$$\frac{\partial P_0(x_1, x_2, \dots, \lambda)}{\partial x_s} + \sum_{r=1}^{N_F} \tilde{x}_r \frac{\partial P_r(x_1, x_2, \dots, \lambda)}{\partial x_s} = 0 ; \quad s = 1, 2, \dots, N_F. \quad (20)$$

These linear equations may now be solved by using a standard decomposition technique for linearly dependent equations, such as the LU decomposition method, once the ket-state correlation coefficients $\{x_r\}$ are known.

Equipped with the above CCM algorithms, which are readily implemented for spin- $\frac{1}{2}$ quantum magnets, we report our new findings on ground-state properties of both the square- and triangular-lattice spin- $\frac{1}{2}$ quantum antiferromagnets in Secs. III and IV, respectively, in order to illustrate the relative simplicity of the present approach. Similar algorithms have also been successfully implemented to study the excitation spectra. This will be the subject of a future publication⁴³.

III. SPIN- $\frac{1}{2}$ XXZ ANTIFERROMAGNET ON THE 2D SQUARE LATTICE

In this section we shall consider the spin- $\frac{1}{2}$ XXZ model on the infinite square lattice. The XXZ Hamiltonian is given by,

$$H = \sum_{\langle i, j \rangle} \left[s_i^x s_j^x + s_i^y s_j^y + \Delta s_i^z s_j^z \right] , \quad (21)$$

where the sum on $\langle i, j \rangle$ runs over all nearest neighbour pairs and counts each pair only once. The square lattice XXZ model has no exact solution, unlike its 1D counterpart, although approximate analytical and numerical calculations have been performed. To put later CCM calculations in context, we note that the XXZ model has three regimes: an Ising-like phase characterised by non-zero Néel order; a planar-like phase in which the spins in the ground-state wavefunction are believed to lie in the xy plane; and a ferromagnetic phase. A Monte Carlo study of the 2D anisotropic Heisenberg model was performed by Barnes *et al.*⁴⁴. They observed that the staggered magnetisation in the z -direction is non-zero for $\Delta > 1$, but then appears to become zero below $\Delta = 1$. They therefore conclude that the critical point is probably very near to this point. In contrast to this Monte Carlo calculation, Kubo and Kishi⁴⁵ have used sum rules to investigate the ground state of this system. They state that the ground state possesses an off-diagonal long-range order (LRO) akin to that of the XY-like state at small anisotropy, $0.0 < \Delta < 0.13$. Also, for $\Delta > 1.78$ they observe that the system demonstrates non-zero Ising-like LRO. At $\Delta = -1$ there is a first-order phase transition to the ferromagnetic phase for this model.

The isotropic Heisenberg point has been extensively studied using various approximate methods, and so shall be used as a test case for the CCM results discussed later in this section. Runge⁴⁰ has performed the most accurate Monte Carlo simulation to date. This provides a value for the ground-state energy per spin of $-0.66934(4)$, and a value for the sublattice magnetisation which is $61.5\% \pm 0.5\%$ of the classical value. In comparison, linear spin-wave theory (LSWT)³⁷ gives a value of -0.658 for the ground-state energy, and a value for the sublattice magnetisation which is 60.6% of the classical value.

A. The Model State

We begin the CCM treatment of this spin system by choosing a suitable model state $|\Phi\rangle$ (for a particular regime), such that all other possible spin configurations may be obtained by the application of linear combinations of products of spin-raising operators to this state. In the Ising-like regime, characterised by non-zero Néel order, a natural choice for the model state is the Néel state with spins lying along the z axis. (For clarity, this state will be referred to as the z -axis Néel model state throughout this article.) We note however that this model state is not the best choice for all values of Δ because the ground-state wavefunction of the XXZ model in the region $-1 < \Delta < 1$ is believed to contain only spins which lie in the xy plane. In this regime, we again use the classical Néel state, but this time with spins lying on the x axis. (This state will be referred to as the planar model state throughout this article.) Hence, we see that even for the same spin model and lattice a different choice of model state may be preferable, depending on the regime that we are investigating.

We shall consider the Ising-like regime first, and, so that spins on either sublattice may be treated equivalently, we perform a rotation of the local axes of the up-pointing spins by 180° about the y axis. The transformation is described by,

$$s^x \rightarrow -s^x, s^y \rightarrow s^y, s^z \rightarrow -s^z. \quad (22)$$

The model state now appears *mathematically* to consist of purely down-pointing spins which is precisely given by Eq. (11), and the Hamiltonian may be written in terms of these local axes as,

$$H = -\frac{1}{2} \sum_{\langle i,j \rangle}^N \left[s_i^+ s_j^+ + s_i^- s_j^- + 2\Delta s_i^z s_j^z \right]. \quad (23)$$

For the planar model state, we again rotate the local axes of these spins on the separate sublattices such that all spins appear to lie along the negative z direction which is again given by Eq. (11). This is achieved by rotating the axes of the left-pointing spins (i.e., those pointing along the negative x direction) in the planar model state by 90° about the y axis, and by rotating the axes of the right-pointing spins (i.e., those pointing along the positive x direction) by 270° about the y axis. (The positive z -axis is defined to point directly upwards, and the positive x -axis is defined to point directly to the right.) Hence the transformation of the local axes of the left-pointing spins is described by,

$$s^x \rightarrow s^z, s^y \rightarrow s^y, s^z \rightarrow -s^x. \quad (24)$$

and the transformation of the local axes of the right-pointing spins is described by,

$$s^x \rightarrow -s^z, s^y \rightarrow s^y, s^z \rightarrow s^x; \quad (25)$$

The transformed Hamiltonian for the planar model state is now given by,

$$H = -\frac{1}{4} \sum_{\langle i,j \rangle}^N \left[(\Delta + 1)(s_i^+ s_j^+ + s_i^- s_j^-) + (\Delta - 1)(s_i^+ s_j^- + s_i^- s_j^+) + 4s_i^z s_j^z \right]. \quad (26)$$

In the remainder of this section, the power and flexibility of our new formalism is illustrated by focussing primarily on the planar model state applied to the XXZ model on the square lattice. Note however that equivalent calculations have been undertaken for the z -axis Néel model state, and that a general explanation is presented here only. A more detailed explanation of CCM calculations that deal with both the ground-state properties and the excitation spectrum using the new formalism for the XXZ model based on this model state will be presented in Ref.⁴³.

B. Fundamental Excitation Configurations: Lattice Animals

As described in Sec. IIB, the first step of our modular solution is to obtain the set of fundamental configurations for a given approximation scheme by utilising appropriate lattice symmetries. Another constructive way to define the LSUB m scheme used here for the square lattice is to consider a right-angled *bounding triangle* containing m lattice points along the sides parallel to the axes (see Fig. 1 for a diagram of this construction where the bounding triangle for LSUB4 is shown). All possible fundamental configurations for the LSUB m approximation are then confined by this bounding triangle. This comes about because it is easy to show that all connected configurations

of size m (or the lattice animals of size m) are constrained to lie within or on this bounding triangle. Furthermore, as first shown by Lunn⁴⁶, the introduction of this bounding triangle greatly simplifies the recursive procedure of *growing* a connected cluster of given size. The disconnected configurations for LSUB m scheme are then constructed by successively considering all “subsets” of each member of the fundamental set of connected configurations, and all possible disconnected configurations are thereby generated. (The “subsets” here refer to all independent configurations which are formed by removing one or more spins from these connected configurations.)

To be specific, for the square lattice, there are four rotational operations, (0° , 90° , 180° , 270°), and four reflections, (along the x and y axes, and along the lines $x=y$ and $x=-y$), which preserve the symmetries of both the lattice and the Hamiltonian. Moreover, the Hamiltonian of Eq. (26), which is defined with respect to the planar model state, contains only even products of spin-flip operators and a single term containing two s^z operators. Repeated application of this Hamiltonian to this model state yields the ground state (assuming that this model state is not orthogonal to it). Therefore the ground state will have an even numbers of spin flips with respect to this model state, and so we restrict the LSUB m approximations to contain even numbers of spin-raising operators in the ket-state correlation operator, S , only for this planar model state. As an example, in Fig. 1 we show all 10 fundamental configurations retained in the LSUB4 approximation when the planar model state is used in the CCM calculation.

Further reduction in the number of fundamental configurations can be made when the z -axis Néel model state is used in the CCM calculations. This comes about because, although the total uniform magnetisation $s_T^z = \sum_i s_i^z$ (where s_i^z is defined with respect to a global quantisation axis and the sum on the index i runs over all lattice sites) is always a good quantum number independent of the model state used, only the z -axis Néel model state is an eigenstate of the total uniform magnetisation s_T^z . In contrast, the planar model state is not an eigenstate of the total uniform magnetisation s_T^z . Therefore, for the z -axis model state case one can explicitly conserve s_T^z by restricting the fundamental configurations to those which produce no change in s_T^z with respect to the z -axis Néel model state. This restriction, for example, reduces the number of the fundamental configurations retained in the LSUB4 approximation to 7 if the z -axis Néel model state is employed in the CCM calculations, and see Fig. 1. We tabulate the number of fundamental configurations up to the LSUB8 level of approximation for both model states in Table I. Note that only the CCM calculations based on the z -axis Néel model state are actually carried out up to LSUB8 approximation in this article.

C. Similarity-transformed Hamiltonian and CCM Ket-State Equations

In order to solve the Schrödinger equation of Eq. (1), we shall specifically utilise the Hamiltonian of Eq. (26), although a comparable analysis can also be performed for Eq. (23). The expression for the ket-state correlation operator of Eq. (12) is now used to write the similarity-transformed Hamiltonian, \hat{H} , of Eq. (10) in terms of the operators F_k and G_{km} . Furthermore, we subdivide \hat{H} into three categories as discussed in Sec. IIB to clarify the problem of finding the CCM equations, where $\hat{H}|\Phi\rangle = e^{-S} H e^S |\Phi\rangle = (\hat{H}_1 + \hat{H}_2 + \hat{H}_3)|\Phi\rangle$, such that:

$$\begin{aligned} \hat{H}_1 &= \frac{1}{2} \sum_{k\rho} \left\{ -(G_{km} + F_k F_m) + \frac{1}{4}(\Delta - 1)(F_m^2 + F_k^2) \right\} s_k^+ s_m^+ \\ &\quad - \frac{1}{8}(\Delta + 1) \sum_{k\rho} \left\{ 2G_{km}^2 + 4G_{km} F_k F_m + F_k^2 F_m^2 \right\} s_k^+ s_m^+ ; \end{aligned} \quad (27)$$

$$\begin{aligned} \hat{H}_2 &= \frac{1}{4} \sum_{k\rho} \left\{ F_m s_m^+ + F_k s_k^+ + \frac{1}{2}(1 - \Delta)(F_m s_k^+ + F_k s_m^+) \right\} \\ &\quad + \frac{1}{8}(\Delta + 1) \sum_{k\rho} \left\{ (2G_{km} + F_k F_m)(F_m s_m^+ + F_k s_k^+) \right\} ; \end{aligned} \quad (28)$$

$$\hat{H}_3 = -\frac{1}{8} \sum_{k\rho} \left\{ 1 + (\Delta + 1)(G_{km} + F_k F_m) \right\} . \quad (29)$$

Note that k runs over all lattice sites and that m is given by $m \equiv k + \rho$, such that ρ covers all nearest neighbours to k . Hence we see from Eq. (29) that the ground-state energy of the XXZ model for the planar model state is given by,

$$\frac{E_g}{N} = -\frac{z}{8} \left[2x_1(\Delta + 1) + 1 \right] , \quad (30)$$

where $x_1 \equiv [k, k+\rho]$ represents all nearest-neighbour, two-body correlation coefficients in Eq. (12) which are equivalent under the translational and rotational symmetries of the lattice, and z represents the lattice coordination number (i.e., the number of nearest neighbours to a given site). Note that the ground-state energy of Eq. (30) is *exact* in the sense that both the exact expansion for S and any non-trivial approximation of it will always produce this expression.

D. Results

1. Ground-State Energy

The ground-state energy for the planar model state is illustrated by Fig. 2, and we can see that these results appear to be in good agreement with Monte Carlo results⁴⁴. The highest approximation that has been attempted for the planar model state is the LSUB6 approximation, which contains 131 fundamental configurations and gives a ground-state energy per spin of -0.66700 at the Heisenberg point. For the z -axis Néel model state, due to the reduced number of fundamental configurations, we were able to solve the LSUB8 approximation, which contains 1287 fundamental configurations and gives an energy per spin of -0.66817 at $\Delta = 1$. Hence, by utilising the new formalism we have increased the number of fundamental configurations used in a CCM calculation for the z -axis Néel model state by over an order of magnitude compared to the previous best (i.e., LSUB6²⁷ which contains 75 configurations). Table I summarises the information regarding numbers of configurations and ground-state energies at $\Delta = 1$. Note that the calculations for both model states at the Heisenberg point give exactly the same results at equivalent approximation levels, and so only one figure for the ground-state energy is quoted in Table I. The reason for the equivalence is that the Hamiltonians of Eqs. (23) and (26) become identical at $\Delta=1$. Also, all of the correlation coefficients for configurations at a given LSUB m level contained in the planar model state case but not contained in the z -axis Néel model state case become identically zero at $\Delta = 1$.

The results for the z -axis Néel model state are found to be less accurate than those using the planar model state in the region $-1 < \Delta < 1$. Conversely, for $\Delta > 1$, the results based on the z -axis Néel model state become the more accurate of the two sets of calculations. This therefore vindicates our decision to use two separate model states in order to investigate the Ising- and planar-like phases of this model.

2. Anisotropy Susceptibility

Beyond certain values of the anisotropy parameter (called critical points) it is found that there is no physically reasonable solution to the LSUB m CCM equations for $m \geq 4$. This characteristic breakdown of the solution CCM equations has previously been related to a phase transition of the real system²⁷. We may also define a quantity called the anisotropy susceptibility, given by,

$$\chi_a \equiv -\frac{\partial^2(E_g/N)}{\partial\Delta^2} , \quad (31)$$

which diverges at the LSUB m critical points. Table I illustrates two sets of estimates for the critical points for the XXZ model based on the planar model state, corresponding to the ferromagnetic and antiferromagnetic phase transition points. Encouragingly, the critical points corresponding to the ferromagnetic phase transition become closer to $\Delta = -1$ with approximation level. Table I also includes the estimates for the critical points obtained for the z -axis Néel model state corresponding to the antiferromagnetic phase transition point. Note that LSUB m results based on these two model states always bound the Heisenberg point, at which the true antiferromagnetic phase transition is believed to lie, and also appear to converge with increasing m .

3. Sublattice Magnetisation

We now consider a simple order parameter called the sublattice magnetisation, $M^+ \equiv -2\langle s^z \rangle$, which is defined in terms of the local, rotated spin axes. Hence M^+ is given by,

$$M^+ = \frac{-2}{N_0} \sum_{i=1}^{N_0} \langle \tilde{\Psi} | s_i^z | \Psi \rangle = 1 - \frac{2}{N_0} \sum_{k=1}^{N_0} \langle \Phi | \tilde{S} F_k s_k^+ | \Phi \rangle = 1 - 2 \sum_{r=1}^{N_F} (n_r)! \tilde{x}_r x_r , \quad (32)$$

where the index i runs over all N_0 sites of a sublattice, and N_F again indicates the total number of configurations for a given LSUB m approximation level. Note that \tilde{x}_r and x_r , respectively, are the bra- and ket-state correlation coefficients associated with the r^{th} fundamental configuration, and that n_r is the number of spins in this configuration. From Eq. (32) we can see that in order to obtain a numerical value for the sublattice magnetisation we must first know the values of both the ket- and bra-state correlation coefficients. The manner in which we determine these coefficients was described in Sec. II. Our results for the XXZ model using the planar model state are shown in Fig. 3, and we note that these results appear to converge to a non-zero value as one increases the approximation level. Hence our results indicate non-zero Néel-type long-range order in the xy plane for the square lattice in the planar regime. Table I also summarises the results for the sublattice magnetisation at the Heisenberg point. Note that results based on both model states are again found to be identical at this point and so only a single number is quoted in Table I.

In summary, the new CCM formalism has been used in order to calculate estimates of the ground-state energy and sublattice magnetisation for the 2D XXZ model, and these results are found to be in good agreement with other approximate calculations. The highest-order approximation for the z -axis Néel model state has been extended to LSUB8 level using the new formalism, which is an increase of over an order of magnitude in the number of fundamental configurations used in the previous-highest LSUB6 calculation. Also, the positions of the phase transition points obtained by the CCM, using both model states, are fully consistent with the known behaviour for this model. Finally, the results presented here also support the idea that this model contains both Ising- and planar-like phases.

IV. SPIN- $\frac{1}{2}$ TRIANGULAR LATTICE ANTIFERROMAGNET

Unlike the square-lattice spin- $\frac{1}{2}$ HAF where various calculations including extensive quantum QMC simulations^{39,40} strongly support the existence of a Néel ordering with a reduced magnetic moment of about 62% of its classical value (See Sec. III), the three-sublattice ordering for the corresponding triangular case is much less clear. For instance, early variational wavefunction calculations⁴¹ that include long-ranged two-spin and nearest-neighbour three-spin correlations support an ordered ground state with a value of sublattice magnetisation, $M^+ = 0.68$, i.e., as large as 68% of the classical value. Based on this antiferromagnetic correlated trial wavefunction, fixed-node Green function Monte Carlo simulations were recently performed on lattices of up to 324 sites⁴⁷. These yielded a similar magnetisation, $M^+ \approx 0.60$ ⁴⁷. However, series expansion calculations¹⁵, utilising up to 11th-order terms in an Ising-like anisotropy parameter suggest that the triangular HAF may be at, or at least close to (with the magnetisation being extrapolated to a value of $M^+ \approx 0.20$), the critical point of losing magnetic order. This scenario has received support from exact diagonalisation calculations on lattices of up to 36 sites⁴⁸. Yet another careful analysis²⁰ of the same data from exact diagonalisations in terms of a consistent description of the symmetries and dynamics of the quasi-degenerate joint states indicates the presence of sublattice magnetic order with the magnetisation value, $M^+ \approx 0.50$, which is also consistent with second-order spin-wave calculations²¹. Clearly, further work is still needed to account for the discrepancy, and to provide a more definite and converged result.

Hence, in this section we therefore further apply the CCM to the spin- $\frac{1}{2}$ triangular HAF and focus on model-specific details of the algorithm implementation discussed in Sec. II. Compared with earlier applications of the CCM on the triangular HAF which only include two-spin (though long-ranged) correlations³³, the current calculations, which take into account all multi-spin correlations on up to six contiguous sites, have obtained various ground-state properties that are now found to be fully competitive with those obtained from the above-mentioned methods.

A. Model Hamiltonian and Model State

The spin- $\frac{1}{2}$ triangular HAF is described by the antiferromagnetic-coupling Hamiltonian,

$$H = \sum_{\langle i,j \rangle} \vec{s}_i \cdot \vec{s}_j \quad , \quad (33)$$

where \vec{s}_i denotes the spin- $\frac{1}{2}$ operator at site i on the infinite triangular lattice. The sum in Eq. (33) on $\langle i, j \rangle$ runs over all nearest-neighbour pairs and counts each pair once. We note that the operators in Eq. (33) are defined in terms of some global spin quantisation axes referring to all spins, whereas henceforth we shall consistently employ a notation in which the spin operators are described in terms of local (Néel-like) quantisation axes for each of the three sublattices (A, B, and C) of the triangular lattice. The classical ground-state of Eq. (33) is the Néel-like state where all spins on each sublattice are separately aligned (all in the xz -plane, say). The spins on sublattice A are oriented along the negative z -axis, and spins on sublattices B and C are oriented at $+120^\circ$ and -120° , respectively, with respect

to the spins on sublattice A. In order both to facilitate the extension of the isotropic Heisenberg antiferromagnet to include an Ising-like anisotropy first introduced by Singh and Huse¹⁵ and to make a suitable choice of the CCM model state, we perform the following spin-rotation transformations. Specifically, we leave the spin axes on sublattice A unchanged, and we rotate about the y -axis the spin axes on sublattices B and C by -120° and $+120^\circ$ respectively,

$$\begin{aligned} s_B^x &\rightarrow -\frac{1}{2}s_B^x - \frac{\sqrt{3}}{2}s_B^z ; & s_C^x &\rightarrow -\frac{1}{2}s_C^x + \frac{\sqrt{3}}{2}s_C^z , \\ s_B^y &\rightarrow s_B^y ; & s_C^y &\rightarrow s_C^y , \\ s_B^z &\rightarrow \frac{\sqrt{3}}{2}s_B^x - \frac{1}{2}s_B^z ; & s_C^z &\rightarrow -\frac{\sqrt{3}}{2}s_C^x - \frac{1}{2}s_C^z . \end{aligned} \quad (34)$$

We may rewrite Eq. (33) in terms of spins defined in these local quantisation axes for the triangular lattice with a further introduction of an anisotropy parameter λ for the non-Ising-like pieces,

$$\begin{aligned} H = \sum_{\langle i \rightarrow j \rangle} &\left\{ -\frac{1}{2}s_i^z s_j^z + \frac{\sqrt{3}\lambda}{4} (s_i^z s_j^+ + s_i^z s_j^- - s_i^+ s_j^z - s_i^- s_j^z) \right. \\ &\left. + \frac{\lambda}{8} (s_i^+ s_j^- + s_i^- s_j^+) - \frac{3\lambda}{8} (s_i^+ s_j^+ + s_i^- s_j^-) \right\} , \end{aligned} \quad (35)$$

where $\lambda = 1$ corresponds to the isotropic Heisenberg Hamiltonian of Eq. (33). We note that the summation in Eq. (35) again runs over nearest-neighbour bonds, but now also with a *directionality* indicated by $\langle i \rightarrow j \rangle$, which goes from A to B, B to C, and C to A. When $\lambda = 0$, the Hamiltonian in Eq. (35) describes the usual classical Ising system with a unique ground-state which is simply the fully aligned (“ferromagnetic”) configuration in the local spin coordinates described above. We choose this state as the uncorrelated CCM model state $|\Phi\rangle$ which is, of course, precisely given by Eq. (11).

B. Fundamental Excitation Configurations: Lattice Animals

Unlike the square lattice case discussed in Sec. IIIB where all lattice point-group symmetries are employed to produce symmetry-distinct configurations, care must be exercised here since not all of the lattice point-group symmetries leave the lattice-spin Hamiltonian invariant. The Hamiltonian of Eq. (35) (or the CCM model state) explicitly breaks some of the lattice symmetries because of the presence of bond-directionality in the Hamiltonian. Thus only 6 (instead of the full 12) point-group symmetries should be used in the symmetry reduction. These are, specifically, three rotational operations (0° , 120° , and 240°) together with three reflections about the lattice axes (i.e., lines that coincide with the edges of the triangular lattice). For example, the three configurations (a), (b), and (c) shown in Fig. 4 are symmetry equivalent, as are the three configurations (d), (e), and (f). However, the former are regarded as inequivalent to the latter in the context of the present spin-lattice Hamiltonian problem. For the purpose of comparison with the case in, say, percolation problems, and for the sake of concreteness, let us consider the connected configurations of size 6. If all 12 point-group symmetries were used, we would have obtained 82 symmetry-inequivalent configurations as shown in Fig. 5, which are further classified into two groups: 17 in group A and 65 in group B. The configurations in group A are of higher symmetries than those in group B, and thus do not lead to new symmetry-inequivalent configurations when only 6 point-group symmetries must be used in the symmetry reduction as discussed above. Each configuration in group B, however, results in another new symmetry-inequivalent configuration. Therefore, the total number of symmetry-inequivalent connected configurations of size 6 is 147 for the present spin-Hamiltonian problem. The set of symmetry-inequivalent configurations (connected and disconnected) thereby forms the set of fundamental configurations. We tabulate the number of fundamental configurations up to the LSUB7 level of approximation in Table II. Note that only CCM computations up to the LSUB6 level of approximation are actually carried out in this article.

C. Similarity-Transformed Hamiltonian and CCM Ket-State Equations

Using Eq. (15) given in Sec. IIIB, we can straightforwardly carry out the similarity transformation of the Hamiltonian given by Eq. (35); the resulting terms are further classified into three categories for reasons already discussed in Sec. IIIB, i.e., $\hat{H}|\Phi\rangle \equiv e^{-S} H e^S |\Phi\rangle = (\hat{H}_1 + \hat{H}_2 + \hat{H}_3)|\Phi\rangle$, as indicated below:

$$\begin{aligned} \hat{H}_1 = & \frac{1}{4} \sum_{k\rho} \left\{ -2(G_{km} + F_k F_m) - \frac{3\lambda}{2} + \sqrt{3}\lambda(F_k - F_m)(1 + 2G_{km} + F_k F_m) \right\} s_k^+ s_m^+ \\ & + \frac{1}{4} \sum_{k\rho} \left\{ -\frac{\lambda}{2}(F_m^2 + F_k^2) - 3\lambda G_{km}^2 - 6\lambda G_{km} F_k F_m - \frac{3\lambda}{2} F_k^2 F_m^2 \right\} s_k^+ s_m^+ ; \end{aligned} \quad (36)$$

$$\begin{aligned} \hat{H}_2 = & \frac{1}{4} \sum_{k\rho} \left\{ [F_m - \frac{\sqrt{3}\lambda}{2}(1 - F_m^2) + \frac{\lambda}{2} F_k] s_m^+ + [F_k + \frac{\sqrt{3}\lambda}{2}(1 - F_k^2) + \frac{\lambda}{2} F_m] s_k^+ \right\} \\ & + \frac{1}{4} \sum_{k\rho} \left\{ \sqrt{3}\lambda(G_{km} + F_k F_m)(s_k^+ - s_m^+) + \frac{3\lambda}{2}(2G_{km} + F_k F_m)(F_m s_m^+ + F_k s_k^+) \right\} ; \end{aligned} \quad (37)$$

$$\hat{H}_3 = \frac{1}{4} \sum_{k\rho} \left\{ -\frac{1}{2} - \frac{\sqrt{3}\lambda}{2}(F_m - F_k) - \frac{3\lambda}{2}(G_{km} + F_k F_m) \right\}. \quad (38)$$

Here the summation over k runs over all triangular lattice sites, while the summation over ρ is over the three directed nearest-neighbour vectors that point from A to B, B to C, and C to A as required by the explicit bond directionality in the Hamiltonian given by Eq. (35), and the index $m \equiv k + \rho$. Each fundamental configuration for a given LSUB m approximation is then *pattern-matched* to each of the total 35 terms in the above similarity-transformed Hamiltonian following the procedure outlined in Sec. IIB to generate the entire set of coupled CCM ket-state equations. The CCM ket-state equations may then be solved by the Newton-Raphson method for nonlinear equations. Specifically, we start from the point $\lambda = 0$, at which we know the exact solution where all the correlation coefficients are zero. We then use this known solution as an initial input in solving the CCM equations for a slightly increased nonzero anisotropy λ . This procedure is carried out recursively to obtain the numerical results reported below.

D. Results

1. Ground-State Energy

In Fig. 6 we show the ground-state energy per spin E_g/N as a function of the anisotropy parameter λ for various LSUB m approximations. The corresponding values at the isotropic Heisenberg point are also tabulated in Table II. The highest-order calculation, LSUB6, which consists of 758 independent fundamental correlation coefficients, yields $E_g/N = -0.54290$. This value should be compared with the value -0.5445 extrapolated from finite-cluster diagonalisations of up to 36-spin clusters¹⁸, and the value -0.5431 ± 0.0001 from a recent QMC simulation⁴⁷. Compared with the corresponding classical value of -0.375 , it is safe to say that the LSUB6 CCM calculation captures at least 99% of the quantum corrections. Due to the lack of rigorous finite-size scaling results, the investigation of which itself presents an interesting and important open question, no attempt at extrapolation is made here. Nonetheless, the ground-state energy obtained from the LSUB6 approximation alone is fully competitive with those obtained from the above-mentioned alternative methods, and is clearly among the best estimates currently available.

To make further contact with the highest-order series expansion known to date¹⁵, we have computed the perturbative solution of E_g/N in terms of the anisotropy parameter λ . In Table III we tabulate the expansion coefficients from the LSUB6 approximation, together with the corresponding results from exact series expansions¹⁵. We note that the LSUB6 approximation reproduces the exact series expansion up to the 6th order. This result lends further strong support to the conjecture that the LSUB m approximation reproduces the *exact* series expansion to the same m th order⁴⁹. Moreover, the fact that the corresponding values of several of the higher-order expansion coefficients from both the CCM LSUB6 perturbative solution and the exact series expansion remain close to each other shows that the exponential parametrisation of the CCM with the inclusion of multi-spin correlation up to certain order also captures the dominant contributions to correlations of a few higher orders in the series expansions. Further detailed series analysis, using such methods as Padé approximant techniques, for the perturbative expansions of both the ground-state energy E_g/N and the sublattice magnetisation M^+ will be reported elsewhere⁵⁰.

2. Anisotropy Susceptibility

As already displayed in Fig. 6, the LSUB m ground-state energy curve for $m \geq 3$ terminates at lower and upper critical values of the anisotropy, λ_{c_1} and λ_{c_2} respectively, beyond which no physical solution of the CCM ket-state

equations exists. We have also tabulated λ_{c_1} and λ_{c_2} for various LSUB m approximations in Table II. Although the CCM based on the model state given in Eq. (11) with the three-sublattice magnetic ordering is bound to break down in the region of the anisotropy parameter space where the true ground-state wavefunction possesses a different symmetry from that of the model state, it has been strongly argued^{23,26} that the terminating points may correspond to the critical points of a phase transition. In order to shed further light on the nature of the terminating points, we investigate the singular behaviour of the CCM correlation coefficients near these points by calculating the derivatives of these coefficients with respect to the anisotropy parameter. Specifically, we display in Fig. 7 the anisotropy susceptibility defined analogously to Eq. (31) as, $\chi_a \equiv -\partial^2(E_g/N)/\partial\lambda^2$. Clearly, χ_a diverges at the corresponding terminating anisotropy parameters λ_{c_1} and λ_{c_2} . Note that the lower terminating point λ_{c_1} clearly converges to a value of about -0.5 , as argued by Singh and Huse¹⁵. However, the upper terminating point λ_{c_2} , as tabulated in Table II, remains considerably larger than the value of unity which was obtained via Padé analysis of the series expansion by Singh and Huse¹⁵. Further work is needed to explain this disagreement and also to determine the singularity exponents of the ground-state energy at the two critical points.

3. Sublattice Magnetisation

Once the ket- and bra-state correlation coefficients are known it is possible to evaluate the sublattice magnetisation, $M^+ \equiv -2\langle s^z \rangle$, which is similarly defined by Eq. (32) except that the subscript i now covers all N_0 sites on the sublattice A, one of the three sublattices. In Table II we also tabulate the sublattice magnetisations at the Heisenberg point for the various LSUB m approximations. The highest-order LSUB6 approximation gives give rise to a value of 0.6561, which agrees well with the corresponding value of 0.60 obtained recently from QMC simulations⁴⁷. However, the discrepancy with that from finite-size and the second-order spin-wave calculations still needs to be accounted for.

The divergence in $\langle s^z \rangle$ seen in Fig. 8 near the critical points is a natural consequence of the approximate nature of the calculation. As we approach a critical point for a given LSUB m approximation, one of the CCM correlation coefficients x_r becomes very large. The contribution to $\langle s^z \rangle$ from this coefficient also becomes very large and so the sublattice magnetisation diverges. The puzzling ‘‘upturn’’ of M^+ observed for the LSUB5 and the LSUB6 approximations near their respective upper critical points λ_{c_2} remains elusive to us at the present.

In summary, compared with earlier applications of the CCM on the triangular HAF which have already revealed interesting oscillatory behaviour in long-ranged two-spin correlations³³, the present high-order CCM calculations (with a systematic inclusion of multi-spin correlations on up to six contiguous lattice sites) have already obtained results including ground-state energy and sublattice magnetisation that are fully competitive with those obtained from other methods, and which are among the best available. Further detailed analysis of the large number of ket-state coefficients already obtained for the LSUB6 approximation, in order to achieve a better understanding of the nodal surface of the ground-state wavefunction, may provide a more microscopic justification of, and an extension to, the above-mentioned variational wavefunction. This may in turn lead to a better trial wavefunction for QMC simulations.

V. CONCLUSIONS AND OUTLOOK

In conclusion to this article, we restate the main points of the new formalism, and discuss the results for the two spin models to which it has been applied. We also consider the future development of the CCM using the new approach, and make suggestions regarding possible strategies in order to extend the CCM calculations to even higher orders.

Our new formalism has reformulated the Hamiltonian purely in terms of spin-raising operators acting on some suitable model state. We note that the reduction in CPU processing time is realised by cutting out one large task, namely, the evaluation of the similarity transform. Also, the method presented here largely negates the task of checking for double occupancy for the spin- $\frac{1}{2}$ system, which can also cause considerable delay. The simple and straightforward nature of the terms within the similarity-transformed Hamiltonian means that one may easily amend the code in our programs to deal with other systems and lattices, and so we have a very flexible approach.

We have seen that the ground-state energy results for both of the systems considered are fully competitive with QMC energies, without recourse to large computing facilities; we have used a HP series 700 workstation containing 96 Megabytes of RAM to perform the calculations presented here. We have also seen that sublattice magnetisations have been determined which are again fully competitive with QMC calculations.

The present limitations of the new method arise from two sources. One limitation is that we must save our CCM equations in memory or on disk in order to obtain expectation values. The rapid increase in the number of fundamental configurations with increasing LSUB m approximation level means that the cost in memory and disk space rapidly becomes prohibitive, and the task of solving the CCM equations becomes slower also. Another limitation is that, as

discussed in Sec. IIB, we search over a wide area in order to determine the ‘free’ indices within specific terms in \hat{H} . In 1D, we find that this area depends on m linearly, but in 2D, for example, this area increases quadratically with m . We need to perform this search because, as yet, we do not take into account the manner in which the members of the set of fundamental configurations are inter-related. For example, some configurations are related to others by the addition or subtraction of a single spin. Thus, most of the processing time is spent sweeping through this area regardless of whether we know that a particular configuration will contribute or not. A useful gain could be to determine the way in which the configurations are related, using graph theory⁵¹ for example, and then to use this knowledge in order to reduce the search area.

We have seen that the CCM LSUB6 approximation fully reproduces the first 6 coefficients of the exact series expansion for the triangular HAF. Also, for higher orders in the series than sixth order, it is found that the CCM captures about 99% of the expansion coefficient of the 7th order, and about 75% of those of higher orders up to 11th order in the ground-state energy perturbation series on the triangular lattice. CCM expansions of the ground-state energy have also been performed up to sixtieth order, at a fraction of the computational cost compared to a direct calculation of the exact series to this order. A possible way of overcoming the memory and disk space limit, when finding the CCM equations, is to derive a perturbative solution to the CCM equations (as previously discussed in Sec. IV). We obtain the expansion coefficients of the ket-state correlation coefficients in terms of powers of some coupling parameter. As shown in Table III, we may then substitute the series expansions for the ket-state correlation coefficients into the ground-state energy equation, thus forming a power series for this quantity in powers of the coupling parameter. The prospective gain is that we might use less disk space in evaluating and storing the series coefficients than in storing the CCM equations. However, each CCM equation must be evaluated many times in order to determine the power series, which in turn means that we must significantly increase the speed of our code. We note that the number of LSUB m configurations that is needed in order to reproduce exact n^{th} -order perturbation theory is a small fraction of the total number of LSUB m configurations. Hence, if one can state beforehand which configurations are necessary in order to reproduce n^{th} -order perturbation theory, an elegant method of reducing the processing time and memory overheads might be to use this small fraction instead of the total number of LSUB m configurations.

Another exciting prospect in order to increase the speed might be to generate the CCM equations *in parallel*. Also, the CCM is well suited to parallelisation as each CCM equation could be implemented on a separate processor. Note that the evaluation of each equation depends only on the target configuration and the form of the Hamiltonian, which remains constant. The possible weaknesses of this approach are that one is limited not only by the number of nodes in the system, but more importantly also by the ‘weakest link’. By this we mean that one can only progress as fast as the evaluation of the slowest equation at each iteration. However, very large gains are possible by sharing out the processing needs.

To recap, we have mentioned that our results using the new CCM formalism are now fully competitive with QMC results, and we have seen that our approach is easily generalisable to other systems. Possible future systems to which we may apply the new formalism include the valence-bond solids^{31,36}, systems with higher spin^{28,29}, and models with electronic degrees of freedom such as the Hubbard model⁵². The nature of the ground states of new and interesting materials or spin models might be quickly and easily investigated by specifying the Hamiltonian, lattice and spin number, and development of the code might therefore lead to a powerful test-bench for various new ideas. The future also holds the possibility of very high-order calculations, which will increase our knowledge both of these systems and also of the CCM. With the inclusion of very high orders of approximation it is also hoped that the asymptotic nature of the CCM ground-state energies, sublattice magnetisations and phase transitions will become clear. In conclusion, we believe that the application of the CCM to the lattice spin systems is yielding excellent and interesting results, though there are still many avenues of fruitful and challenging research to be investigated.

VI. ACKNOWLEDGEMENTS

We thank J.B. Parkinson and N.R. Walet for their interesting and useful discussions. C. Zeng gratefully acknowledges support from NSF grant DMR-9419257 at Syracuse University, and R.F. Bishop gratefully acknowledges a grant from the Engineering and Physical Sciences Research Council (EPSRC) of Great Britain.

* Present address: Department of Physics, Syracuse University, Syracuse, NY 13210, USA.

[†] E-mail address: R.F.Bishop@UMIST.AC.UK

- ¹ F. Coester, *Nucl. Phys.* **7**, 421 (1958); F. Coester and H. Kümmel, *ibid.* **17**, 477 (1960).
- ² J. Čížek, *J. Chem. Phys.* **45**, 4256 (1966); *Adv. Chem. Phys.* **14**, 35 (1969).
- ³ R.F. Bishop and K.H. Lührmann, *Phys. Rev. B* **17**, 3757 (1978).
- ⁴ H. Kümmel, K.H. Lührmann, and J.G. Zabolitzky, *Phys Rep.* **36C**, 1 (1978).
- ⁵ J.S. Arponen, *Ann. Phys. (N.Y.)* **151**, 311 (1983).
- ⁶ R.F. Bishop and H. Kümmel, *Phys. Today* **40(3)**, 52 (1987).
- ⁷ J.S. Arponen, R.F. Bishop, and E. Pajanne, *Phys. Rev. A* **36**, 2519 (1987); *ibid.* **36**, 2539 (1987); in *Condensed Matter Theories*, edited by P. Vashishta, R.K. Kalia, and R.F. Bishop (Plenum, New York, 1987), Vol. 2, p. 357.
- ⁸ R.J. Bartlett, *J. Phys. Chem.* **93**, 1697 (1989).
- ⁹ R.F. Bishop, *Theor. Chim. Acta* **80**, 95 (1991).
- ¹⁰ F.D.M. Haldane, *Phys. Lett.* **93A**, 464 (1983); *Phys. Rev. Lett.* **50**, 1153 (1983).
- ¹¹ S.R. White and D.A. Huse, *Phys. Rev. B* **48**, 3844 (1993).
- ¹² V. Kalmeyer and R.B. Laughlin, *Phys. Rev. Lett.* **59**, 2095 (1987); *Phys. Rev. B* **39**, 11879 (1989).
- ¹³ C. Zeng and V. Elser, *Phys. Rev. B* **42**, 8436 (1990).
- ¹⁴ J.T. Chalker and J.F.G. Eastmond, *Phys. Rev. B* **46**, 14201 (1992).
- ¹⁵ R.R.P. Singh and D.A. Huse, *Phys. Rev. Lett.* **68**, 1766 (1992).
- ¹⁶ S. Sachdev, *Phys. Rev. B* **45**, 12377 (1992).
- ¹⁷ K. Yang, L.K. Warman, and S.M. Girvin, *Phys. Rev. Lett.* **70**, 2641 (1993).
- ¹⁸ B. Bernu, C. Lhuillier, and L. Pierre, *Phys. Rev. Lett.* **69**, 2590 (1992).
- ¹⁹ N. Elstner and A.P. Young, *Phys. Rev. B* **50**, 6871 (1994).
- ²⁰ B. Bernu, P. Lecheminant, C. Lhuillier, and L. Pierre, *Phys. Scripta* **T49**, 192 (1993); *Phys. Rev. B* **50**, 10048 (1994).
- ²¹ R. Deutscher, H.V. Everts, S. Miyashita, and M. Wintel, *J. Phys. A.: Math. Gen.* **23**, L1043 (1990); R. Deutscher and H.V. Everts, *Z. Phys. B: Condensed Matter* **93**, 77 (1993).
- ²² M. Roger and J.H. Hetherington, *Phys. Rev. B* **41**, 200 (1990).
- ²³ R.F. Bishop, J.B. Parkinson, and Y. Xian, *Phys. Rev. B* **43**, 13782 (1991); *Theor. Chim. Acta* **80**, 181 (1991); *Phys. Rev. B* **44**, 9425 (1991); in *Recent Progress in Many-Body Theories*, edited by T.L. Ainsworth, C.E. Campbell, B.E. Clements, and E. Krotscheck (Plenum, New York, 1992), Vol. 3, p. 117.
- ²⁴ F.E. Harris, *Phys. Rev. B* **47**, 7903 (1993).
- ²⁵ F. Cornu, Th. Jolicoeur, and J.C. Le Guillou, *Phys. Rev. B* **49**, 9548 (1994).
- ²⁶ R.F. Bishop, R.G. Hale, and Y. Xian, *Phys. Rev. Lett.* **73**, 3157 (1994).
- ²⁷ R.F. Bishop, R.G. Hale, and Y. Xian, *Phys. Rev. B* **46**, 880 (1992).
- ²⁸ W.H. Wong, C.F. Lo, and Y.L. Wang, *Phys. Rev. B* **50**, 6126 (1994).
- ²⁹ R.F. Bishop, J.B. Parkinson, and Y. Xian, *J. Phys.: Condens. Matter* **5**, 9169 (1993).
- ³⁰ D.J.J. Farnell and J.B. Parkinson, *J. Phys.: Condens. Matter* **6**, 5521 (1994).
- ³¹ Y. Xian, *J. Phys.: Condens. Matter* **6**, 5965 (1994).
- ³² R. Bursill, G.A. Gehring, D.J.J. Farnell, J.B. Parkinson, T. Xiang, and C. Zeng, *J. Phys.: Condens. Matter* **7**, 8605 (1995).
- ³³ C. Zeng, I. Staples, and R.F. Bishop, *J. Phys.: Condens. Matter* **7**, 9021 (1995); *Phys. Rev. B* **53**, 9168 (1996).
- ³⁴ C. Zeng and R.F. Bishop, in *Coherent Approaches to Fluctuations*, edited by M. Suzuki and N. Kawashima, (World Scientific, Singapore, 1996), p. 296.
- ³⁵ C.F. Lo, K.K. Pang, and Y.L. Wang, *J. Appl. Phys.* **70**, 6080 (1991).
- ³⁶ Y. Xian, in *Condensed Matter Theories*, edited by M. Casas, M. de Llano, and A. Polls (Plenum, New York, 1995), Vol. 10, p. 541.
- ³⁷ P.W. Anderson, *Phys. Rev.* **86**, 694 (1952); T. Oguchi, *ibid.* **117**, 117 (1960).
- ³⁸ R.R.P. Singh, *Phys. Rev. B* **39**, 9760 (1989); W. Zheng, J. Oitmaa, and C.J. Hamer, *ibid.* **44**, 11869 (1991).
- ³⁹ J. Carlson, *Phys. Rev. B* **40**, 846 (1989); N. Trivedi and D.M. Ceperley, *ibid.* **41**, 4552 (1990).
- ⁴⁰ K.J. Runge, *Phys. Rev. B* **45**, 12292 (1992); *ibid.* **45**, 7229 (1992).
- ⁴¹ D.A. Huse and V. Elser, *Phys. Rev. Lett.* **60**, 2531 (1988).
- ⁴² S. Mertens, *J. Stat. Phys.* **58**, 1095 (1990).
- ⁴³ D.J.J. Farnell, C. Zeng, J.B. Parkinson, and R.F. Bishop, *unpublished*.
- ⁴⁴ T. Barnes, D. Kotchan, and E. S. Swanson, *Phys. Rev. B* **39**, 4357 (1989).
- ⁴⁵ K. Kubo and T. Kishi, *Phys. Rev. Lett.* **61**, 2585 (1988).
- ⁴⁶ W.F. Lunnon, in *Graph Theory and Computing*, edited by R.C. Read (Academic Press, New York, 1972), p. 87.
- ⁴⁷ M. Boninsegni, *Phys. Rev. B* **52**, 5304 (1995).
- ⁴⁸ P.W. Leung and K. Runge, *Phys. Rev. B* **47**, 5861 (1993).
- ⁴⁹ R.F. Bishop, J.B. Parkinson, and Y. Xian, *J. Phys.: Condens. Matter* **4**, 5783 (1992).
- ⁵⁰ C. Zeng, D.J.J. Farnell, and R.F. Bishop, *unpublished*.
- ⁵¹ B. Flaming, *Practical Data Structures in C++*, (Coriolis Group Book, Wiley, New York, 1993), p. 281.
- ⁵² M. Roger and J.H. Hetherington, *Europhys. Lett.* **11**, 255 (1990); C.F. Lo, E. Manousakis, and Y.L. Wang, *Phys. Lett. A* **156**, 42 (1991); F. Petit and M. Roger, *Phys. Rev. B* **49**, 3453 (1994); R.F. Bishop, Y. Xian, and C. Zeng, *Int. J. Quantum*

Chem. **55**, 181 (1995).

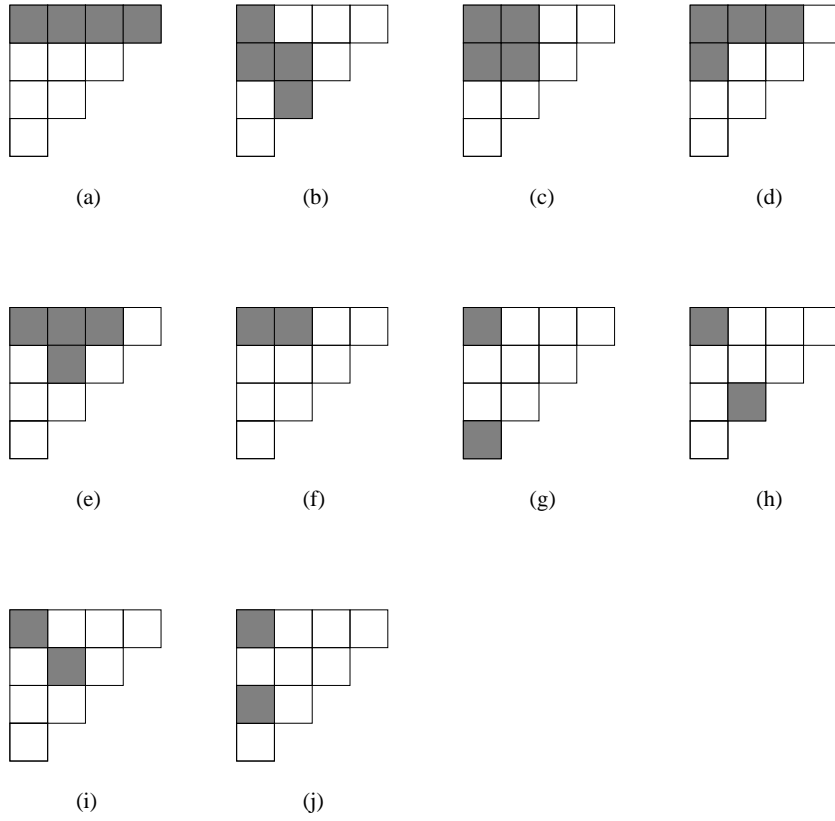


FIG. 1. The square lattice LSUB4 bounding triangle is shown in this figure along with the LSUB4 lattice animals, illustrated by diagrams (a)-(e). The fundamental LSUB4 configurations for the planar model state are given by diagrams (a)-(j), and the fundamental configurations for the z -axis Néel model state form a subset of them, namely, all diagrams except (e), (i), and (j). The centres of the shaded squares mark the relative positions of the sites of the square lattice on which the spins are flipped with respect to the model state.

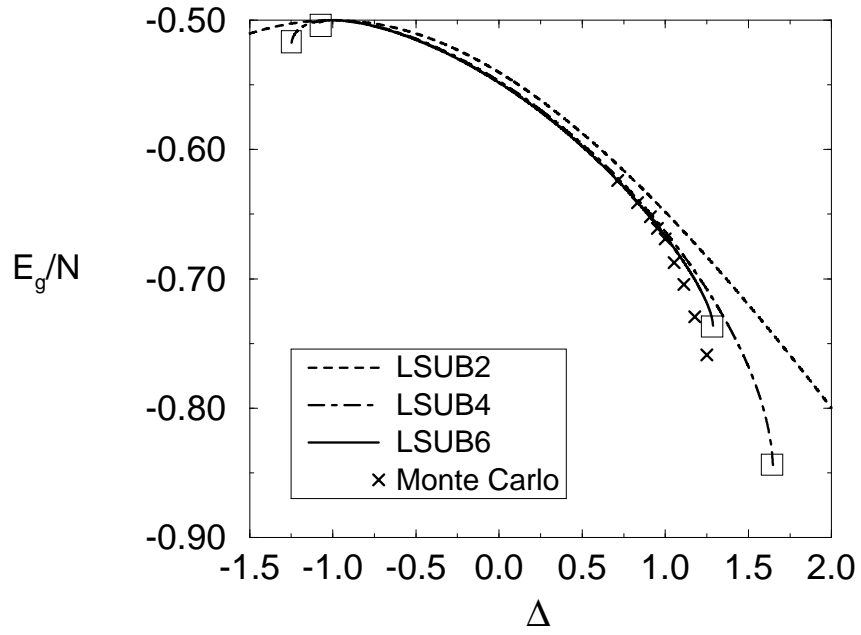


FIG. 2. Results for the CCM ground-state energy of the XXZ model on the 2D square lattice using the planar model state, compared to the Monte Carlo results of Ref. [44]. $LSUBm$ critical Δ_{c_1} and Δ_{c_2} points are indicated by the boxes.

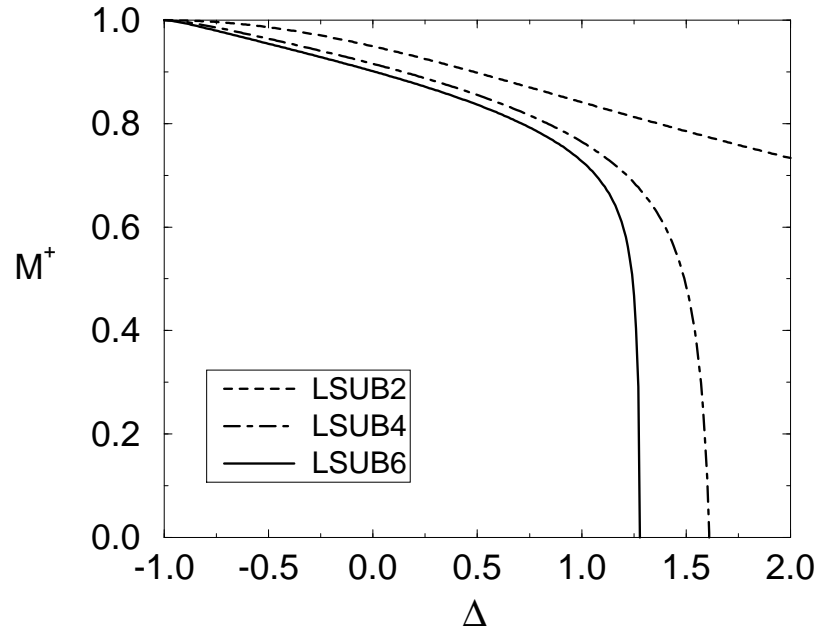


FIG. 3. Results for the CCM sublattice magnetisation of the XXZ model on the 2D square lattice using the planar model state. CCM results indicate non-zero, in-plane long-range order in the region $-1 < \Delta < 1$.

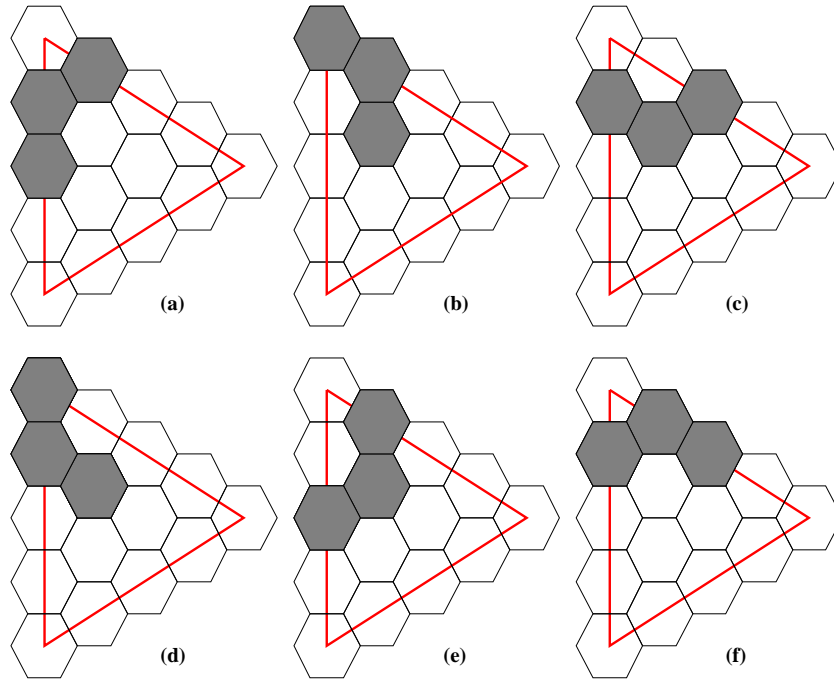


FIG. 4. The LSUB5 bounding triangle and symmetry-related correlation configurations for the triangular lattice. The centres of the shaded hexagons mark the relative position of the sites of the triangular lattice on which the spins are flipped with respect to the model state. See text for details.

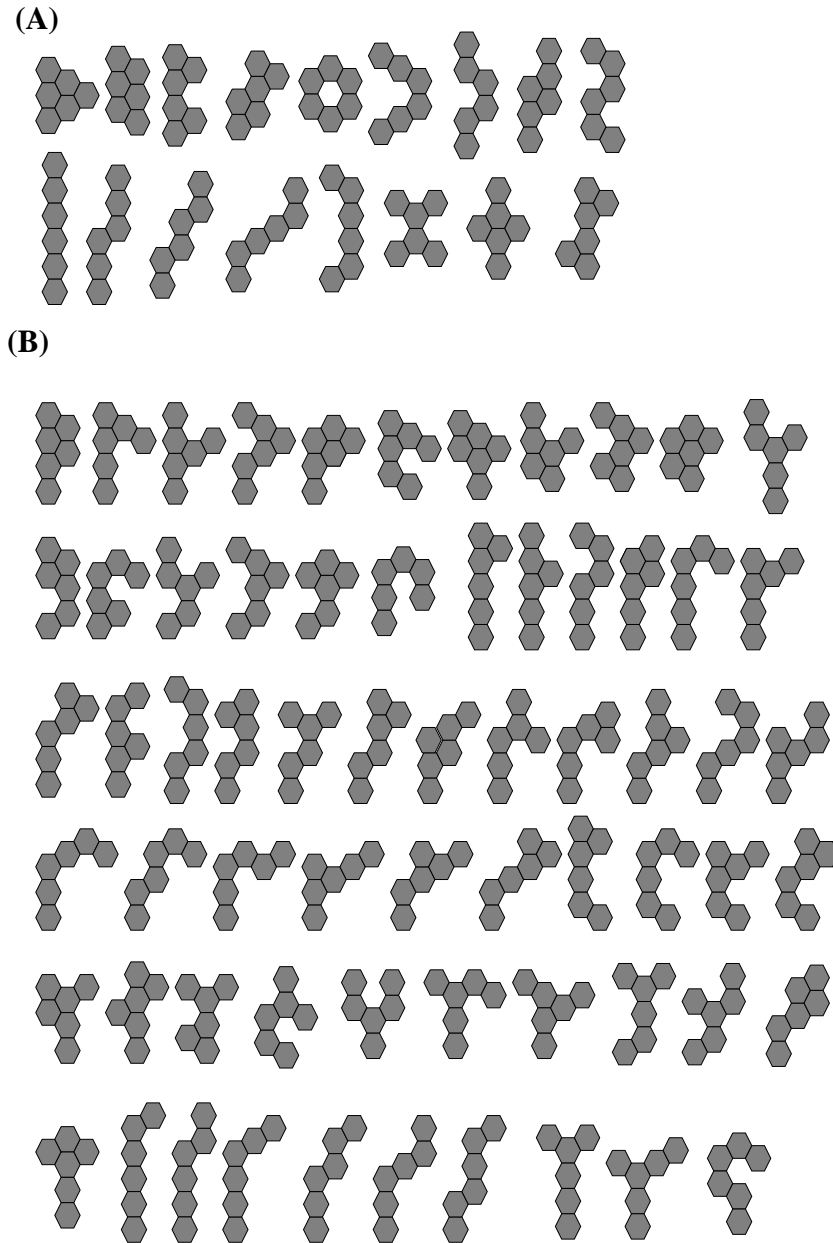


FIG. 5. All 82 lattice animals of size 6 on a triangular lattice after symmetry reduction including translational and 12 point-group symmetry operations (see text for details). The centres of the hexagons mark the relative position of the sites of the triangular lattice on which the spins are flipped with respect to the model state. See text for a discussion of group A and group B diagrams.

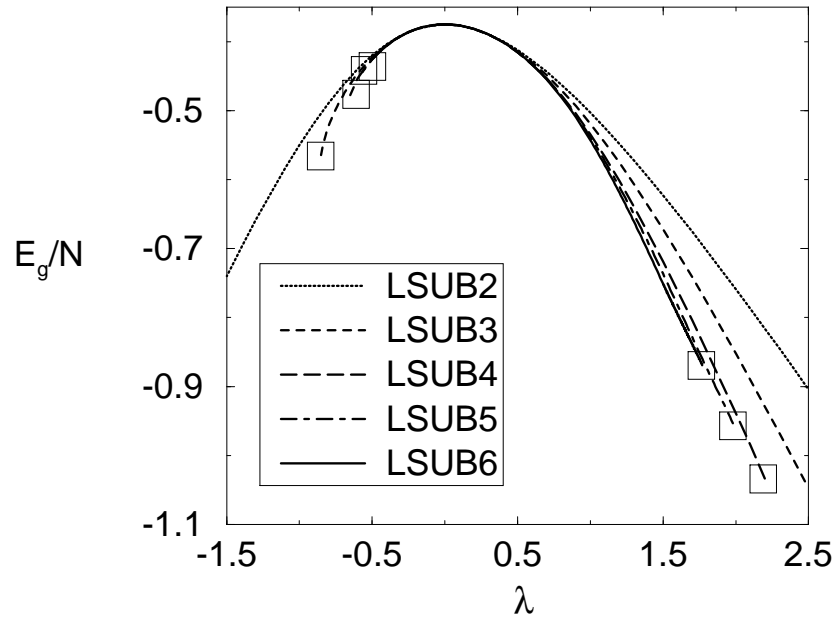


FIG. 6. Results for the CCM ground-state energy for the triangular HAF. LSUB m critical points λ_{c_1} and λ_{c_2} are indicated by the boxes.

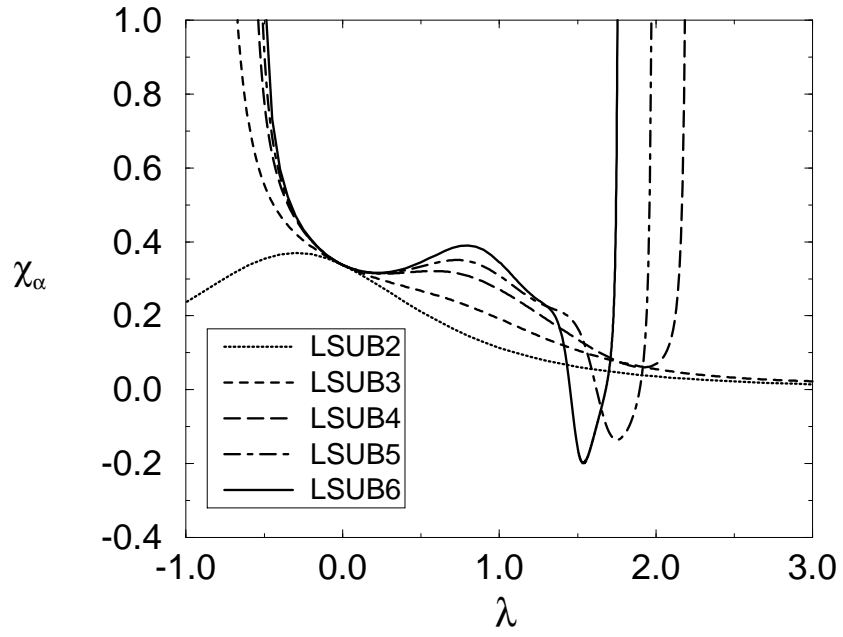


FIG. 7. Results for the CCM ground-state anisotropy susceptibility for the triangular HAF.

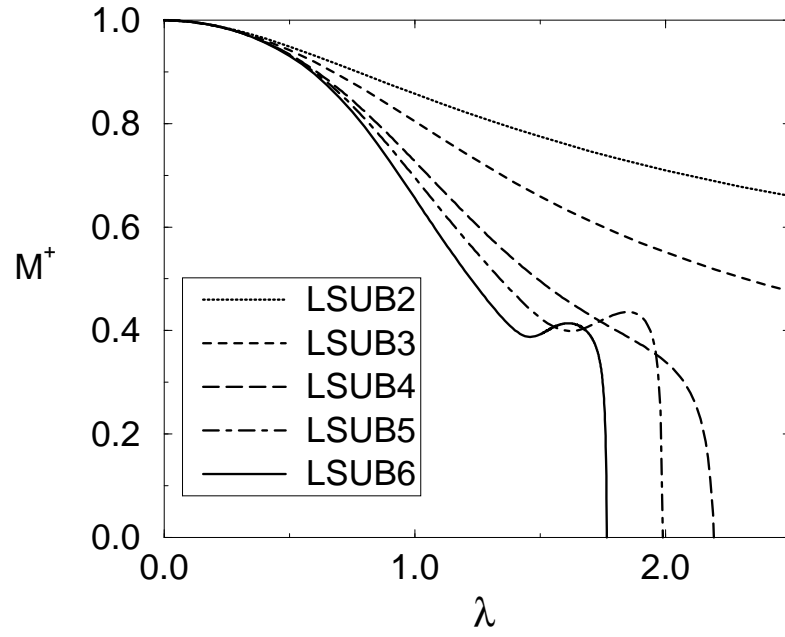


FIG. 8. Results for the CCM ground-state sublattice magnetisation for the triangular HAF.

TABLE I. Results obtained for the spin- $\frac{1}{2}$ XXZ model on the 2D square lattice using CCM LSUB m approximations ($m = 2, 4, 6, 8$). N_{F_1} denotes the number of fundamental configurations for the planar model state, which are further decomposed in terms of connected and disconnected ones respectively, and N_{F_2} denotes the number of fundamental configurations for the z -axis Néel model state. The ground-state energy per spin, E_g/N , and the sublattice magnetisation, M^+ , at the isotropic Heisenberg point ($\Delta = 1$) are shown, together with various critical anisotropy parameters. Δ_{c_1} and Δ_{c_2} indicate the LSUB m critical points for the planar model state corresponding to the ferromagnetic and antiferromagnetic phase transitions. Δ_{c_3} indicates the critical point for the z -axis Néel model state corresponding to the antiferromagnetic phase transition. Note that there are no terminating points in the LSUB2 approximation.

m	N_{F_1}	N_{F_2}	E_g/N ($\Delta = 1$)	M^+ ($\Delta = 1$)	Δ_{c_1}	Δ_{c_2}	Δ_{c_3}
2	1 (1+0)	1 (1+0)	-0.64833	0.8414	-	-	-
4	10 (6+4)	7 (5+2)	-0.66366	0.7648	-1.249	1.648	0.577
6	131 (41+90)	75 (29+46)	-0.66700	0.7273	-1.083	1.286	0.7631
8	2793 (410+2383)	1287 (259+1028)	-0.66817	0.7048	?	?	0.8429

TABLE II. Results obtained for the spin- $\frac{1}{2}$ triangular-lattice HAF using CCM LSUB m approximations ($m = 2, 3, 4, 5, 6, 7$). N_F denotes the number of fundamental configurations which are further decomposed in terms of connected and disconnected ones respectively. Note that only CCM calculations up to the LSUB6 level of approximation are performed in this article. The ground-state energy per spin, E_g/N , and the sublattice magnetisation, M^+ , at the isotropic Heisenberg point ($\lambda = 1$) are shown for each LSUB m approximation. The terminating anisotropy parameters, λ_{c_1} and λ_{c_2} , which correspond respectively to a phase transition at $\lambda = -\frac{1}{2}$ and another believed [15] to be near $\lambda = 1$, are also given for each LSUB m approximation. Note that there is no terminating point in the LSUB2 approximation.

m	N_F	E_g/N ($\lambda = 1$)	M^+ ($\lambda = 1$)	λ_{c_1}	λ_{c_2}
2	2 (2+0)	-0.50290	0.8578	-	-
3	8 (6+2)	-0.51911	0.8015	-0.86	5.47
4	30 (16+24)	-0.53427	0.7273	-0.65	2.20
5	143 (53+90)	-0.53869	0.6958	-0.60	1.98
6	758 (200+558)	-0.54290	0.6561	-0.55	1.77
7	4427 (837+3590)	?	?	?	?

TABLE III. Expansion coefficients in powers of λ up to the 15th order for the ground-state energy per spin, E_g/N , for the anisotropic spin- $\frac{1}{2}$ triangular-lattice HAF obtained from the CCM equations in the LSUB6 approximation. The highest-order known exact series expansions up to the 11th order obtained by Singh and Huse [15] are also included for comparison.

Order	LSUB6	Exact
0	-0.3750000	-0.3750000
1	0.0000000	0.0000000
2	-0.1687500	-0.1687500
3	0.0337500	0.0337500
4	-0.0443371	-0.0443371
5	0.0204259	0.0204259
6	-0.0283291	-0.0283291
7	0.0311703	0.0315349
8	-0.0357291	-0.0476598
9	0.0541263	0.0685087
10	-0.0771681	-0.1025446
11	0.1294578	0.1565522
12	-0.1848858	?
13	0.2857225	?
14	-0.4463496	?
15	0.7021061	?